

# SN 2003bg: a broad-lined Type IIb Supernova with Hydrogen

Paolo A. Mazzali<sup>1,2,3,4</sup>, Jinsong Deng<sup>5</sup>, Mario Hamuy<sup>6</sup>, Ken'ichi Nomoto<sup>7</sup>

## ABSTRACT

Models for the spectra and the light curve, in the photospheric as well as in the late nebular phase, are used to infer the properties of the very radio-bright, broad-lined type IIb Supernova 2003bg. Consistent fits to the light curve and the spectral evolution are obtained with an explosion that ejected  $\approx 4M_{\odot}$  of material with a kinetic energy of  $\approx 5 \cdot 10^{51}$  erg. A thin layer of hydrogen, comprising  $\sim 0.05M_{\odot}$ , is inferred to be present in the ejecta at the highest velocities ( $v \gtrsim 9000 \text{ km s}^{-1}$ ), while a thicker helium layer, comprising  $\approx 1.25M_{\odot}$ , was ejected at velocities between 6500 and 9000  $\text{km s}^{-1}$ . At lower velocities, heavier elements are present, including  $\sim 0.2M_{\odot}$  of  $^{56}\text{Ni}$  that shape the light curve and the late-time nebular spectra. These values suggest that the progenitor star had a mass of  $\approx 20 - 25M_{\odot}$  (comparable to, but maybe somewhat smaller than that of the progenitor of the XRF/SN 2008D). The rather broad-lined early spectra are the result of the presence of a small amount of material ( $\approx 0.03M_{\odot}$ ) at velocities  $> 0.1c$ , which carries  $\approx 10\%$  of the explosion kinetic energy. No clear signatures of a highly aspherical explosion are detected.

*Subject headings:* supernovae: general — supernovae: individual (SN 2003bg) — stars: evolution — nucleosynthesis

---

<sup>1</sup>Scuola Normale Superiore, Piazza dei Cavalieri, 7, 56126 Pisa, Italy

<sup>2</sup>National Institute for Astrophysics–OAPd, Vicolo dell’Osservatorio, 5, 35122 Padova, Italy

<sup>3</sup>Max-Planck-Institut für Astrophysik, Karl-Schwarzschildstr. 1, 85748 Garching, Germany

<sup>4</sup>Research Center for the Early Universe, University of Tokyo, Bunkyo-ku, Tokyo 113-0033, Japan

<sup>5</sup>National Astronomical Observatories, CAS, 20A Datun Road, Chaoyang District, Beijing 100012, China

<sup>6</sup>Departamento de Astronomía, Universidad de Chile, Casilla 36-D, Santiago, Chile

<sup>7</sup>Institute for the Physics and Mathematics of the Universe, University of Tokyo, Kashiwa, 5-1-5 Kashiwanoha, Kashiwa, Chiba 277-8568, Japan

## 1. Introduction

Stars with an initial mass exceeding  $8 - 10M_{\odot}$  end their life when their core collapses to a compact remnant and the outer layers are ejected in a powerful explosion, a Supernova (SN). If the outer hydrogen envelope of the star is still in place at the time of the explosion, the SN is characterized by strong H lines and is classified as type II (see Filippenko 1997, for a primer on SN classification). There are however cases when the outer layers of the star have been lost before the explosion. In particular, if the H envelope was lost but the He envelope was retained, the SN shows He lines and is classified as a type Ib, while if both the H and He shells were lost neither H nor He lines are seen and the SN is classified as type Ic. Collectively, the class of stripped-envelope SNe is called SNe Ib/c. Type Ib SNe are rarer than type Ic SNe. These subclasses should not be thought of as rigid separations, but rather as an indication of what is probably a continuum of properties. For example, evidence of residual H lines has been claimed in some SNe Ib (e.g. Deng et al. 2000; Anupama et al. 2005).

The study of stripped-envelope SNe gained momentum with the discovery that some extremely energetic SNe Ic (“hypernovae”: HNe) are linked to Gamma-Ray Bursts (Galama et al. 1998; Iwamoto et al. 1998). Thereafter, various studies of SNe Ib/c have been performed, both of individual SNe [e.g. SN 1999ex (Hamuy et al. 2002); SN 2004aw (Taubenberger et al. 2006)], and systematic (e.g. Matheson et al. 2003; Soderberg et al. 2006).

Some SNe Ib/c have also been found in association with X-ray Flashes (XRF), the softer and weaker versions of GRBs (Heise et al. 2001): the SNe Ic 2006aj (Campana et al. 2006; Pian et al. 2006) and the SN Ib 2008D (Soderberg et al. 2008). While the nature of the XRF is debated in both cases (Campana et al. 2006; Ghisellini et al. 2007; Waxman, Mészáros, & Campana 2007; Soderberg et al. 2008; Mazzali et al. 2008), both SNe turned out to be less energetic explosions than the GRB/SNe, but still significantly more energetic than typical SNe Ib/c (Mazzali et al. 2006, 2008; Tanaka et al. 2009), which release  $\approx 10^{51}$  erg of energy (e.g. Iwamoto et al. 1994; Sauer et al. 2006).

It is now clear that SNe Ic, and to some extent also SNe Ib, show a large spread of properties (e.g. Clocchiatti & Wheeler 1997). Studies of various individual objects have begun to paint a picture where the so-called ‘typical’ SNe Ib/c, such as SN 1994I [e.g. Nomoto et al. (1993, 1994); Wheeler et al. (1994); Filippenko et al. (1995); Richmond et al. (1996)] are just a subset of this extended family. Thus, the definition of typical may need revising. The mass of the progenitor stars of SNe Ib/c is not constrained, except that it must be larger than the minimum mass to reach core collapse ( $8 - 10M_{\odot}$ ), if the progenitor was a single star.

The final fate of massive stars depends mostly on mass, but also on other proper-

ties, such as metallicity, rotation, and magnetic fields (e.g. Fryer 1999; Heger et al. 2003; Woosley & Janka 2005). These dependencies on often poorly known quantities add some uncertainty to the determination of the properties of the progenitor from those of the SN ejecta. Presently, SN Ib/c observations and models indicate that the basic SN properties (e.g. the kinetic energy liberated in the explosion,  $E_K$ , the mass ejected,  $M_{\text{ej}}$ ) are apparently related to the progenitor’s mass (Nomoto et al. 2005). It takes very massive stars ( $M_{ZAMS} \sim 40M_{\odot}$ ), possibly of low metallicity, to make a GRB in a highly aspherical explosion that leaves behind a black hole (Fryer 1999; MacFadyen & Woosley 1999). Less massive stars may still collapse to a black hole, possibly via fallback (Fryer 1999), but not give rise to a GRB [e.g. SNe 2002ap, Mazzali et al. (2002) or 1997ef, Iwamoto et al. (2000); Mazzali et al. (2001)]. At lower masses still [ $M_{ZAMS} \lesssim 22M_{\odot}$ , (Fryer 1999), at least if the effect of rotation is not considered], the star collapses to a neutron star and may eject some material at relativistic velocities, but in this case the relativistic outflow is less energetic and is observed as an X-Ray Flash [e.g. SN 2006aj (Mazzali et al. 2006)]. These less energetic explosions may be less asymmetric (Mazzali et al. 2007; Maeda et al. 2008).

One general feature of SNe Ib/c is that their progenitors must have lost at least the outer hydrogen envelope. If a hydrogen envelope more massive than  $\sim 0.1M_{\odot}$  is left, the star would probably have a RSG structure at the time of core collapse, and the SN light curve would be influenced initially by hydrogen recombination and appear as a type II light curve. Some transitional objects like SN 1993J only had a very small hydrogen envelope, whose presence did not affect the light curve significantly but was responsible for the Type II spectrum this SN displayed early on (Nomoto et al. 1993). Spectroscopically, after an early Type II phase SN 1993J turned to a Type Ib, and is therefore known as an SN I Ib. Only few SNe I Ib have been observed, and little is known about their spread in mass and energy.

Exactly how a star manages to preserve just a thin shell of H is debated. The scenarios are different depending on whether the star was single or a member of an interacting binary. In the former case, a mass loss occurs via a radiatively driven stellar wind (e.g. Weiler et al. 2007; Stockdale et al. 2007). This can be effective at relatively high masses ( $\gtrsim 30M_{\odot}$ ). Stars with masses of  $\sim 27 - 28M_{\odot}$  may end their lives with only a thin H shell left in place (Crockett et al. 2008). Such stars would be classified as WRL or WRH (Smith & Conti 2008). However, this mechanism is much less efficient for less luminous stars. Yet, the inference for events such as SN 1993J is that the progenitor had a mass of  $\approx 15M_{\odot}$ . In this case the latter scenario, binary interaction, seems more appealing. For example, Nomoto et al. (1995) suggest that an SN I Ib is a result of the spiral-in of a low-mass companion into a massive star, which causes the ejection of most of the massive star’s H-rich envelope. This is probably a good scenario to produce an energetic explosion, because it can explain both how

the core gains angular momentum from spiral-in, and how most of the envelope is ejected by spiral-in heating. There is some observational evidence in support of the binary scenario: for SN 1993J a spectroscopic companion has been observed (Maund et al. 2004). Evidence of a binary companion has also been claimed for the SNIb 2001ig (Ryder et al. 2006), while for the SNIb 2008ax Crockett et al. (2008) suggest that binary interaction may be a more viable scenario than that of a single star. A similar debate exists also regarding the origin of SNe Ib/c (e.g. Nomoto et al. 1993, 2001).

SN 2003bg was initially classified as a broad-lined SNIc (Filippenko & Chornock 2003), but it soon developed a broad  $H\alpha$  P-Cygni feature as well as He I lines, making it a SNIb. This is the first SNIb for which broad lines have been observed, suggesting that it is a SNIb hypernova. The optical data of SN 2003bg are presented in a companion paper (Hamuy et al. 2009). In the nebular phase the spectra were similar to those of SNe Ib/c, but evidence of H may be present in the form of a weak, flat-topped  $H\alpha$  emission, reminiscent of SN 1993J. Additionally, SN 2003bg was exceptional for its radio luminosity. Soderberg et al. (2006) suggest that the observed radio light curve can be interpreted as the signature of sub-relativistic ejecta (with velocity  $v \sim 0.2c$ ) producing synchrotron radiation as they impacted into a medium that may have had the properties of a WR-star wind (mass loss rate  $\dot{M} \sim 4 \cdot 10^{-5} M_{\odot} \text{ yr}^{-1}$ , wind velocity  $v \sim 1000 \text{ km s}^{-1}$ ). They also suggest that the wind may have been highly variable, especially just before the explosion. This is reminiscent of the situation of the XRF-SN 2006aj, which was probably surrounded by a thick wind shell [Campana et al. (2006); Waxman, Mészáros, & Campana (2007), but see Ghisellini et al. (2007)]. Interestingly, the radio light curve of SN 2003bg and that of SN 2001ig were very similar.

The available evidence therefore suggests some similarity among all SNeIb, despite clear differences in the ejected mass and the kinetic energy of the explosion: for SN 1993J Nomoto et al. (1993) estimated an ejected mass of  $4M_{\odot}$  and an explosion  $E_K$  of  $10^{51}$  erg, while for SN 2001ig Silverman et al. (2009) estimate an ejected mass of  $\sim 1M_{\odot}$  below a velocity of  $4300 \text{ km s}^{-1}$ .

Here we concentrate on extracting the basic properties of SN 2003bg, and hence of the progenitor star and of the explosion. In order to do this we model the light curve and the spectra in both the early photospheric phase and the late nebular phase.

## 2. Data

Observations of SN 2003bg started very soon after the putative explosion date (2003 Feb 25 UT), and cover the evolution of the SN for almost one year, extending into the nebular phase (see Hamuy et al. 2009, for more details). The peak phase was unfortunately not covered, and there is a gap in the data at the onset of the linear decline phase. Still, the available data make it possible to constrain the properties of the SN reasonably accurately, especially in view of the availability of both early and late spectra.

We have modelled 10 spectra, of which 8 were obtained around the peak and 2 in the nebular phase. Combining the analysis of the outer part of the ejecta conducted by means of the early-time spectra and the determination of the properties of the inner, slow-moving ejecta made possible by the nebular spectra, both the density and the abundance stratification in the SN ejecta can be determined.

## 3. Models for the early phase

Unlike Type Ia SNe, the modelling of SNe Ib/c must establish both  $E_K$  and  $M_{ej}$  simultaneously. As these are the two parameters that play the major role in determining both the light curve and the spectra, clearly a reliable solution must be able to reproduce simultaneously both the spectral evolution and the light curve. As is well known, the solution of the light curve alone is degenerate to  $E_K$  and  $M_{ej}$  if both are allowed to vary (Arnett 1982), as is the case for SNe Ib/c.

The first steps to obtaining a solution are therefore to consider that: i) the light curve has a rather narrow peak: the presence of H and He does not influence the light curve much, because the H shell must be thin and He does not contribute significantly to the opacity. ii) the earliest spectra have broad lines, similar to but not quite as broad as SN 2002ap (Mazzali et al. 2002). iii) the brightness of SN 2003bg at peak suggests that it synthesized  $\sim 0.2M_{\odot}$  of  $^{56}\text{Ni}$ . This is more than in ‘normal’ SNe Ib/c, and comparable to non-GRB hypernovae such as SNe 1997ef or 1997dq (Mazzali et al. 2004), and the XRF-SNe 2006aj (Mazzali et al. 2006) or 2008D (Mazzali et al. 2008; Tanaka et al. 2009).

### 3.1. Method

The early-time spectra were modelled using a Monte Carlo radiative transfer code (Mazzali & Lucy 1993; Lucy 1999; Mazzali 2000). The code assumes that the SN luminosity

emerges from a sharp, grey photosphere (Schuster-Schwarzschild approximation). This approximation is valid if most  $\gamma$ -rays and positrons produced in the radioactive decay of  $^{56}\text{Ni}$  to  $^{56}\text{Co}$  and hence to  $^{56}\text{Fe}$  deposit their energy, which is eventually thermalised and converted into optical photons, below the photosphere. This is the case in the early phases of a Type I SN. Using as input the SN luminosity and the velocity of the photosphere at the desired epoch of the model (velocity and time give the photospheric radius since the expansion of SN ejecta is homologous:  $v = rt$ ), an approximate effective temperature at the photosphere can be obtained assuming black body emission ( $L = 4\pi R^2 \sigma_B T^4$ , where  $\sigma_B$  is Stefan-Boltzmann's constant).

Photons emitted at the photosphere propagate in the expanding ejecta, where radiative equilibrium is assumed. Photons can undergo electron scattering and they can interact with spectral lines. In the latter case, photon branching is explicitly considered (Lucy 1999; Mazzali 2000). This process allows photons to shift from wavelengths where line opacity is very high to spectral regions where line opacity is low, and thus to escape the SN envelope, and it is essential in shaping the spectra of Type I SNe. Level populations and the ionization structure in the SN envelope are computed taking into account deviations from Local Thermodynamic Equilibrium (LTE) using a nebular approximation as discussed in Abbott & Lucy (1985) and Mazzali & Lucy (1993). This approximation has been shown to reproduce well the effects of non-LTE (Pauldrach et al. 1996). Iterating a series of MC experiments, a temperature structure in the ejecta is then computed. Finally, the emerging flux is recorded using an efficient formal integral approach (Lucy 1999). The calculation of the observed flux requires the values of the distance and the reddening to the SN. The code has been applied to a number of Type I SNe (e.g. Mazzali et al. 2008).

Apart from the parameters described above, and for atomic models, the only other input required by the code is the run of density in the ejecta with expansion velocity. This is known as an explosion model. The properties of the model determine the appearance of the spectra. The basic quantities that define an explosion model are the ejected mass and the kinetic energy of the explosion. In particular, the presence of large amounts of material at high velocities leads to spectra characterized by broad lines (Mazzali, Iwamoto, & Nomoto 2000), while, given the same kinetic energy, more massive models have broader light curves (Arnett 1982). The simultaneous fit of the light curve and the spectra of an SN using one explosion model therefore constitutes a validation of the model itself.

Because of the spectral similarity with SNe 1997ef and 2002ap we started with an explosion model based on CO100, a model characterized by  $M_{\text{ej}} \sim 8M_{\odot}$  and  $E_K \sim 10^{52}$  erg. Model CO100 was used to reproduce the light curve and the spectral evolution of SN 1997ef, but the very broad lines observed in this SN required the addition of a high-velocity, low-

density tail which increased the  $E_K$  to  $\sim 2 \cdot 10^{52}$  erg. The model was also used in rescaled form (1/4 of the mass) to fit the SN Ic 2002ap, which was characterized by broad spectral features but a relatively narrow light curve (Mazzali et al. 2002). SN 2003bg poses a similar problem. In order to reproduce its narrow light curve we needed to rescale model CO100 down in mass. Furthermore, line blending in SN 2003bg is less extreme than in SNe 1997ef or 2002ap - it is more similar to SN 2006aj: e.g. the Ca II IR triplet and the O I 7774 Å line do not blend - and so the density gradient in the outer part must have been steeper. Therefore we did not need the high-velocity tail, and we finally used a model with half the mass of the original CO100. The model we selected has  $M_{\text{ej}} \sim 4M_{\odot}$  and  $E_K \sim 5 \cdot 10^{51}$  erg.

In the spectral models the luminosity  $L$ , which is a required input, was determined such as to match the flux in the spectra. Another required input is the photospheric velocity  $v_{ph}$ . This was chosen so that the position of the absorption lines and the overall spectral distribution in the synthetic spectra reproduced the observations as closely as possible. The abundances in the ejecta, also a required input, were chosen to optimize the fit, but our aim was not so much to reproduce the details of the spectra but rather to explain the general evolution of the SN.

Because H and He lines appear in the spectra we assumed that these elements are present in the outer part of the ejecta. He lines are notoriously not visible unless the levels of He I are non-thermally excited (Lucy 1991). Non-thermal excitation is caused by the fast electrons which are produced in the thermalization process of the  $\gamma$ -rays that are emitted by the radioactive decay of  $^{56}\text{Ni}$  into  $^{56}\text{Co}$  and hence into  $^{56}\text{Fe}$ , which is the source of light for SNe. At early times, the density in the ejecta is high and thermalization occurs near the place where the  $\gamma$ -rays are emitted. Since the helium layer is located at a larger radius than the  $^{56}\text{Ni}$  non-thermal processes do not occur. Only at later times do fast electrons begin to travel considerable distances before being thermalized. In fact, He I lines develop rather late in SNe Ib (e.g. SN 2008D, Mazzali et al. 2008).

We do not explicitly treat the propagation of the fast electrons, which also requires a detailed mapping of the distribution of  $^{56}\text{Ni}$  in what may have been an aspherical explosion. Therefore, the departure coefficients caused by non-thermal processes with respect to the level population computed with our pseudo-NLTE treatment are not explicitly computed. Instead, we mimic the effect of overexcitation and ionization caused by non-thermal processes using an arbitrary ‘non-thermal factor’  $f_{\text{HeI}}$  to multiply all He I excited level populations. These factors increase with time (Mazzali & Lucy 1998), reflecting the increasing penetration of fast electrons in the SN envelope, and they were taken to be similar to those derived by Lucy (1991). While this is a rough treatment, it gives one at least a feeling for the presence or lack of He in the ejecta (Tominaga et al. 2005). A non-thermal factor was also used for

hydrogen ( $f_{\text{H}}$ ): since the H mass must be small, this was required to match the observed line strengths.

The explosion date was chosen to be 2003 February 25. This gives a rise time to maximum of  $\sim 15 - 20$  days, similar to SN 1998bw. We used a distance modulus of 31.68 ( $d = 24$  Mpc), and a very small reddening [ $E(B - V) = 0.02$ ]. The early-time spectral fits are presented in Figures 1 and 2 and are briefly discussed in the following. The input values for the spectral models are summarized in Table 1.

## 3.2. Results

### 3.2.1. 2003 Feb. 28

The model is shown in Figure 1a. It was computed using  $\log L = 41.47$  [ $\text{erg s}^{-1}$ ],  $v_{ph} = 22000 \text{ km s}^{-1}$ , and  $t = 3$  days. The mass above the photosphere is  $\approx 0.2M_{\odot}$ , and the radiation temperature at the photosphere is  $\sim 7000$  K. Although He dominates the composition (90% by mass above the photospheric velocity), and a non-thermal factor  $f_{\text{HeI}} = 10^3$  was introduced, no strong He lines are visible, and so the He distribution cannot be constrained. Hydrogen is present only in a very small amount (4% by mass). If more H is included, the increased electron density changes the ionization balance of all other species. Therefore, the same non-thermal excitation factor as for He I was used also for H I ( $f_{\text{H}} = 10^3$ ). Both H and He lines make only a minor contribution to the troughs near 6000 and 4300 Å, which are dominated by Si II and Co II lines, respectively. Other features are due to Fe II, Si II, O I, Ca II, and Mg II and are marked in Figure 1a. The presence of a small amount of material at high velocity ( $\approx 0.03M_{\odot}$ ) are located at  $v > 0.1c$  is sufficient to give rise to broad lines.

### 3.2.2. 2003 March 2

The model shown in Figure 1b was computed with  $\log L = 41.82$  [ $\text{erg s}^{-1}$ ],  $v_{ph} = 18000 \text{ km s}^{-1}$ , and  $t = 5$  days. It is similar to the previous one, but the lines are deeper as the photosphere moved rapidly inwards. The mass above the photosphere is now  $\approx 0.4M_{\odot}$ . The abundances are also similar, with He the dominant species. The higher  $L$  leads to a higher radiation temperature near the photosphere,  $T \sim 7500$  K. Hydrogen lines now make an important contribution: in the feature near 6200 Å,  $\text{H}\alpha$  is as strong as Si II 6355 Å, which contributes to making that feature broad. The same non-thermal factors as for Feb 28 ( $f_{\text{HeI}} = 10^3$ ,  $f_{\text{H}} = 10^3$ ) were used for both H I and He I. He I lines are present in the



spectrum. He I 5686 Å is blended with Na I D, which is however weaker. The inconsistent strength of H $\alpha$ , which is too strong, and H $\beta$ , which is comparable to the observation, may suggest that a full, rather than a parametrized treatment of NLTE and non-thermal effects for at least H may be required. If the contribution of Si II 6355 Å to the H $\alpha$ -Si II feature is reduced, the synthetic line does not match the velocity of the observed absorption.

### 3.2.3. 2003 March 4

This model is shown in Figure 1c. It was computed with  $\log L = 41.95$  [erg s $^{-1}$ ],  $v_{ph} = 14100$  km s $^{-1}$ , and  $t = 7$  days. It has a similar composition as the previous model, and the same non-thermal factors for H I and He I ( $f_{HeI} = 10^3$ ,  $f_H = 10^3$ ). As the temperature continues to increase (now  $T \sim 8000$  K) with the luminosity, and more mass (now  $\approx 0.7M_{\odot}$ ) is located above the photosphere, the H and He lines make an increasingly important contribution. H $\alpha$  is now stronger than Si II 6355 Å, H $\beta$  is visible, and so are some of the He I lines (especially 4471 Å and 5876 Å). Apart from this, there are no major differences with respect to the previous spectrum.

### 3.2.4. 2003 March 12

This is the spectrum nearest the time of maximum, the epoch of which was not covered. It was computed with  $\log L = 42.31$  [erg s $^{-1}$ ],  $v_{ph} = 8800$  km s $^{-1}$ , and  $t = 15$  days, and it is shown in Figure 1d. The spectrum is now bluer than before, but the lines are the same. The temperature has further increased ( $T \sim 8600$  K), and now H I and He I lines dominate (the composition is similar to the previous epochs, despite the much larger mass located above the photosphere,  $\approx 1.5M_{\odot}$ , and the same non-thermal factors were used for both H I and He I:  $f_{HeI} = 10^3$ ,  $f_H = 10^3$ ), while Fe makes a smaller contribution by comparison.

### 3.2.5. 2003 March 31

This spectrum was obtained after an observational gap near the time of maximum. It is much redder than all pre-maximum spectra, which is the result of the decrease in temperature ( $T \sim 6000$  K) and luminosity. The model was computed with  $\log L = 42.29$  [erg s $^{-1}$ ],  $v_{ph} = 6000$  km s $^{-1}$ , and  $t = 34$  days, and it is shown in Figure 2a. The mass above the photosphere is now  $\approx 2.4M_{\odot}$ . The abundances are not very different, with a slight decrease of He, which is reduced to  $\sim 70\%$  and replaced mostly by Ne near the photospheric

layers. The abundance of Fe-group elements has now increased to  $\sim 4\%$ , which is required to block the near-UV flux.

Several He I lines are now clearly visible, emphasizing the IIb nature of the SN. They can be reproduced using  $f_{\text{HeI}} = 10^6$ . An increase with time of the departure coefficients can be expected because of the increased penetration of the  $\gamma$ -rays, as discussed by Mazzali & Lucy (1998). Although any statement about the He mass is made highly uncertain by the presence of the huge non-thermal correction, the strength of the He lines suggests that the He mass should be large. In any case, the He-shell is limited to  $\sim 2M_{\odot}$  at most stellar masses in evolutionary models (Nomoto & Hashimoto 1988).

The H I lines are now narrower, and have a smaller blueshift than lines of other elements. In order to get a reasonable match to these lines (only  $\text{H}\alpha$  and  $\text{H}\beta$  are seen) it must be assumed that H is present only at  $v \gtrsim 9000 \text{ km s}^{-1}$ . The non-thermal coefficient is only marginally larger than at previous epochs ( $f_{\text{H}} = 2 \cdot 10^3$ ). Given the low abundance of H (less than 4%), we derive a total H mass of  $\sim 0.05M_{\odot}$ . The mass of H cannot be much larger for two reasons. Firstly, if the mass was much larger than  $0.1M_{\odot}$  the star would not be compact and one would expect a type II light curve, with a phase dominated by H recombination. Secondly, a large H mass would imply a higher electron density, which would then result in a different overall ionization regime and in a worse fit to the spectra. The oxygen abundance near the photosphere cannot be determined because the spectra do not cover the O I 7774 Å line, so the same value as in the previous epoch was used (3%).

### 3.2.6. 2003 April 4

This spectrum was obtained just a few days later and is similar to the previous one. The model (Figure 2b) was computed with  $\log L = 42.24 \text{ [erg s}^{-1}\text{]}$ ,  $v_{ph} = 5600 \text{ km s}^{-1}$ , and  $t = 38$  days. The mass above the photosphere is now  $\approx 2.5M_{\odot}$ , and the temperature has decreased only slightly, to 5600 K. The lines are now more clearly separated, with metal lines making a larger contribution to the spectrum, although  $\text{H}\alpha$ ,  $\text{H}\beta$ , and some He lines are still very strong. The abundances have not changed much. The non-thermal coefficient for He is larger ( $f_{\text{HeI}} = 10^7$ ), but comparable to what was used in Tominaga et al. (2005). The non-thermal coefficient for H is the same as in the previous epoch ( $f_{\text{H}} = 2 \cdot 10^3$ ). H is present only above  $9000 \text{ km s}^{-1}$ , but now a confinement for He has also been introduced at  $6500 \text{ km s}^{-1}$ . This is required to fit the shape and position of the He I lines.

### 3.2.7. 2003 April 9

The next spectrum is similar to the previous one. The model (Figure 2c) was computed with  $\log L = 42.21$  [erg s<sup>-1</sup>],  $v_{ph} = 5100$  km s<sup>-1</sup>, and  $t = 43$  days, and has a mass above the photosphere of  $\approx 2.65M_{\odot}$ . The spectrum is marginally cooler than the previous one ( $T \approx 5300$  K, but the lines that are present are the same. H I and He I lines are sharp. The abundances have changed considerably with respect to the previous spectrum. The abundance of He is down to  $\sim 50\%$  by mass, and O, Ne, and Si are highly abundant near the photosphere. The confinements of H (above 9000 km s<sup>-1</sup>) and He (above 6500 km s<sup>-1</sup>) are as in the previous spectrum, but the non-thermal factors are higher:  $f_{\text{HeI}} = 10^9$  and  $f_{\text{H}} = 3 \cdot 10^3$ . Departure coefficients that increase with time are expected as  $\gamma$ -rays propagate more efficiently (Mazzali & Lucy 1998), but the precise values should be tested with realistic calculations. These require a detailed knowledge of the distribution of <sup>56</sup>Ni as well as of its mass, and are postponed to future work. Still, a slower rise of the non-thermal factor for H I than for He I may be justified by the fact that hydrogen is located further out than helium in the ejecta, and hence it is more separated from the source of fast electrons. Also, H I levels are separated by smaller energies than those of He I, and thus are more coupled to the thermal pool. This also applies to the ionization potentials of the two ions.

### 3.2.8. 2003 April 10

This is the last of the photospheric epoch spectra. The model (Figure 2d) was computed with  $\log L = 42.20$  [erg s<sup>-1</sup>],  $v_{ph} = 5000$  km s<sup>-1</sup>, and  $t = 44$  days. The composition, non-thermal factor and confinements are the same as in the previous spectrum, which was only one day earlier. The mass above the photosphere is now  $\approx 2.7M_{\odot}$ , and the temperature is  $\approx 5300$  K. H I and He I lines are very sharp. The volume sampled by last few spectra in the photospheric epoch is just outside the volume sampled by the nebular spectra.

## 3.3. Results of early-phase modelling

The main result of the photospheric-epoch models are that SN 2003bg was a very energetic explosion (a hypernova) and that H and He are both present, but are clearly confined in velocity: H above 9000 km s<sup>-1</sup> and He above 6500 km s<sup>-1</sup>. This explains the weakness of the H and He lines in the early spectra and the almost complete absence of H in the nebular spectra: these elements are removed from <sup>56</sup>Ni, the source of the fast particles responsible for non-thermal processes. Thus the SN looked like an SNIc early on, although H and He

dominate the composition of the outer ejecta. This is because the H content should be small (only  $\sim 0.05M_{\odot}$ ) and the He I levels giving rise to the strongest lines are not excited early on. These levels are excited mostly via non-thermal processes, but the fast particles that are responsible for the excitation are produced deeper in the ejecta, and cannot penetrate from the deeper regions when the densities are still too high. The delayed development of He lines has been observed before in SNeIb [e.g. SN 2005bf (Anupama et al. 2005); SN 2008D (Soderberg et al. 2008; Mazzali et al. 2008; Tanaka et al. 2009)]. Below  $6500 \text{ km s}^{-1}$ , silicon and oxygen dominate the composition, and Fe-group elements are also significant.

This behaviour of the H I and He I lines shows that if H and He are present in the ejecta they will at some point manifest themselves in the spectra. Since in SNeIc He lines are never seen (e.g. Taubenberger et al. 2006), and H lines are not seen in most SNeIb, these two subtypes must contain very little He and H, respectively.

### 3.4. Models for the nebular phase

In order to assess the properties of the inner parts of the ejecta, and thus to determine both the  $^{56}\text{Ni}$  mass (in addition to the light curve results) and the ejected mass, it is essential that late-phase spectra are modelled as well as early-time ones. At advanced epochs, the SN ejecta become optically thin and behave like a nebula. The gas is heated by the deposition of the  $\gamma$ -rays and positrons that are emitted in the decay of  $^{56}\text{Co}$  to  $^{56}\text{Fe}$ . Collisions of the fast particles that are produced in the thermalization process excite the gas, which is cooled via mostly forbidden-line emission. The gas conditions are modelled with a non-local thermodynamic equilibrium (NLTE) code (Axelrod 1980; Ruiz-Lapuente & Lucy 1992; Mazzali et al. 2001).

The late-time spectra of SNeIb/c are dominated by a strong O I 6300, 6363 Å emission line, the shape of which can be used to infer the geometry of the ejecta and our orientation, thanks to the transparency of the nebula (Mazzali et al. 2005).

We modelled the two latest spectra of SN 2003bg, obtained on 2003 Dec 16 and 23, corresponding to fiducial epochs of 293 and 300 days, respectively. The two spectra are rather similar. Besides O I 6300, 6363 Å, other strong lines are Mg I] 4570 Å, several [Fe II] lines which testify to the brightness of the SN, and Ca II lines.

The shape of the emission lines does not suggest the presence of strong asymmetries, and the spectra can be modelled assuming a single density and homogeneous abundances below a velocity of  $5000 \text{ km s}^{-1}$ , as indicated by the width of the strongest emission lines ([O I], Mg I]). Models for the two spectra yield reasonably consistent results (Fig. 3).

Given the somewhat uncertain flux calibration we take the mean of the results of the two spectral fits. The spectra can be reproduced assuming an emitting mass of  $\approx 1.6M_{\odot}$  located below a velocity of  $5000 \text{ km s}^{-1}$ . The main constituent of the emitting nebula is oxygen ( $\sim 0.9M_{\odot}$ ). Other elements are C ( $\approx 0.1M_{\odot}$ ), Si ( $\approx 0.3M_{\odot}$ ), S ( $\approx 0.1M_{\odot}$ ), Ca ( $\approx 0.02M_{\odot}$ ), Mg ( $\approx 0.005M_{\odot}$ ), and  $^{56}\text{Ni}$ . The mass of  $^{56}\text{Ni}$  in the nebula is  $\approx 0.16M_{\odot}$ , as required by the simultaneous fit of the [Fe II] and other lines. By the time the nebular spectra were observed most  $^{56}\text{Ni}$  had decayed to  $^{56}\text{Co}$  and  $^{56}\text{Fe}$ .

The explosion model we used for the early-time models has a mass of  $1.3M_{\odot}$  below  $5000 \text{ km s}^{-1}$ . The result from the nebular spectra is slightly larger, indicating the presence of more mass at low velocities than included in a spherically symmetric explosion model. This is often seen in SNe Ib/c [e.g. SN 1994I (Sauer et al. 2006); SN 1998bw (Mazzali et al. 2001; Maeda et al. 2002)], and may be the result of some asphericity in the explosion (Maeda & Nomoto 2003), which is typical of HNe and possibly of all core-collapse SNe (Leonard et al. 2006; Maeda et al. 2008). Indeed, a hint for the presence of an inner core of material with higher density may be found in the profile of the [O I] 6300, 6363 Å line, which may be composed of a main profile characterized by narrowly separated double peaks plus a central core and is reminiscent of that of SN 2002ap (Mazzali et al. 2007). A model including a density discontinuity to reproduce this profile in detail may have a slightly smaller total mass. Still, the fact that the deviation from parabolic profiles is very small in all lines suggests that any asphericity is small and probably affects only the innermost ejecta.

The strength of the semi-forbidden Ca II] 7200 Å line with respect to the allowed Ca II IR triplet suggests that the density was low. In our models, the electron density is  $n_e \sim 2 \cdot 10^6 \text{ cm}^{-3}$ . A weak, broad [O I] 5557 Å line may be present in the data, and is only partially reproduced in the synthetic spectra, which also suggests a slightly higher density. A weak, broad emission to the red of [O I] 6300, 6363 Å may be identified as  $\text{H}\alpha$ , as in SN 1993J (Patat, Chugai, & Mazzali 1995).

### 3.5. Results of spectral modelling

Combining the early- and late-time modelling results we find that a model of a highly energetic explosion which ejected  $\sim 4 - 5M_{\odot}$  of material with  $E_K \approx 5 \cdot 10^{51} \text{ erg}$  can reproduce the observations. Only a small mass of H is present,  $\sim 0.05M_{\odot}$ , located at  $v > 9000 \text{ km s}^{-1}$ . A massive He shell is located at  $v > 6500 \text{ km s}^{-1}$ , comprising  $\sim 1 - 2M_{\odot}$ . The ejected CO core mass is  $\sim 3M_{\odot}$ , of which  $\sim 1.3M_{\odot}$  is oxygen. The rest is mostly carbon ( $\sim 0.15M_{\odot}$ ), neon ( $\sim 0.5M_{\odot}$ ), silicon ( $\sim 0.6M_{\odot}$ ), and sulphur ( $\sim 0.2M_{\odot}$ ). The mass of  $^{56}\text{Ni}$  is  $\sim 0.17M_{\odot}$ , most of which is located inside of  $5000 \text{ km s}^{-1}$ . The confinement of  $^{56}\text{Ni}$  to the lowest velocities

explains the late excitation of the He lines.

Layers of H and He at the highest ejecta velocities were found by Branch et al. (2002) in most SNe Ib. In SN 2003bg and in other SNe Ib the H mass must be larger, so that it gives rise to strong spectral lines. Also, in the case of SN 2003bg, we find that H extends deeper than in most SNe Ib, similar to the type IIb SN 1993J (Patat, Chugai, & Mazzali 1995). The inner distribution of helium is at the lower limit of the Branch et al. (2002) sample.

Early on, neither H nor He lines are clearly detected. An elegant explanation of this behaviour of H was given by Branch et al. (2002). Additionally, in the case of SN 2003bg, the early identification of H lines is rendered difficult by the breadth of the spectral features. He lines only develop later, as non-thermal excitation increases with time (see Mazzali & Lucy 1998).

The velocity evolution of SN 2003bg (Figure 4) is similar to that of other SNe Ib/c, in particular the HN SN 2002ap, although our estimate of the explosion epoch is uncertain. It is also similar to SN 2008D early on. The velocities we derived are based on modelling the spectra, and are therefore influenced by trying to reproduce both the overall spectral distribution and the observed line width. Therefore, they are sensitive to the assumed epoch, especially at the earliest phases. This is an indirect way of assessing the reliability of our choice of epoch. If the date of explosion was chosen to be earlier than assumed here, the velocity required to fit the spectra would most likely be smaller, and the synthetic lines would be less blended. A later epoch of explosion, on the other hand, would result in even larger velocities, especially at the earliest times, and the blueshift of the lines would be too large.

#### 4. Light Curve Model

We synthesized the bolometric light curve (LC) of the ejecta models as constrained by spectral fitting, and compare them to the observed LC, which is described in the accompanying paper (Hamuy et al. 2009). We used the 1-D SN LC code that was originally developed by Iwamoto et al. (2000). The code solves the energy and momentum equations of the radiation plus gas in the co-moving frame, and is accurate to first order in  $v/c$ . Electron densities and the electron scattering opacity are determined from the Saha-Boltzmann equation. The energy deposition from radioactive decays of the newly synthesized  $^{56}\text{Ni}$  and its daughter  $^{56}\text{Co}$  is calculated with a gray  $\gamma$ -ray transfer code, assuming an absorptive opacity of  $0.05Y_e \text{ cm}^2 \text{ g}^{-1}$  (Swartz, Sutherland & Harkness 1995). Unlike the sophisticated but time-consuming recipes in the original code, we adopted the approximation proposed by Gómez-Gomar &

Isern (1996) for the Eddington factors, and fitted the TOPS opacities (Magee et al. 1995) to find an empirical relationship between the Rosseland mean and the electron scattering opacity. Such simplifications were also made by the authors when modeling the LCs of other Type Ic SNe.

The best-fitting model LC shown in Fig. 5 (*solid line*) is characterized by an ejected mass of  $\sim 4.8M_{\odot}$ , with a kinetic energy of  $\approx 5 \cdot 10^{51}$  erg and including  $0.15M_{\odot}$  of  $^{56}\text{Ni}$ , whose distribution in the ejecta was adjusted by hand. The density structure above  $5000 \text{ km s}^{-1}$  was obtained scaling model CO100 as constrained by our photospheric-epoch spectral models. Below  $5000 \text{ km s}^{-1}$ , the density was enhanced to the level required by the nebular spectrum modelling. In order to retain the calculation accuracy, the ejecta material with  $v/c > 0.1$  was cut out. This amounts to a negligible mass because of the extremely low density at such high velocities. Except for  $^{56}\text{Ni}$ , we adopted the abundance distribution of other elements derived from the spectrum synthesis. In particular, H exists only at  $v \gtrsim 9000 \text{ km s}^{-1}$ . The total H mass is only  $\approx 0.05 M_{\odot}$ , which is too small to affect the LC shape by H recombination, = as expected. The model LC shown has a  $^{56}\text{Ni}$  distribution of  $\approx 0.01M_{\odot}$  (or  $\approx 1\%$  in mass fraction) between  $10,000$  and  $20,000 \text{ km s}^{-1}$ ,  $\approx 0.04M_{\odot}$  ( $\approx 2.5\%$ ) between  $5,000$  and  $10,000 \text{ km s}^{-1}$ ,  $\approx 0.05M_{\odot}$  ( $\approx 4.4\%$ ) between  $3,000$  and  $5,000 \text{ km s}^{-1}$ , and  $\approx 0.05M_{\odot}$  ( $\approx 4.4\%$ ) below  $3,000 \text{ km s}^{-1}$ . Thus the total  $^{56}\text{Ni}$  mass derived from the light curve ( $0.15M_{\odot}$ ) is similar to that obtained from the spectral fits, but the distribution is different. The light curve model requires more  $^{56}\text{Ni}$  at high velocities.

For comparison, two other model LCs with different model parameters are also shown in Fig. 5. The *dashed line* shows a LC obtained with the same density structure and hence the same mass and kinetic energy as the best-fit LC, but with the  $^{56}\text{Ni}$  distribution derived from the spectrum modelling. The total  $^{56}\text{Ni}$  mass is then  $\approx 0.18M_{\odot}$ , of which  $\approx 0.16M_{\odot}$  are located below  $5000 \text{ km s}^{-1}$ . This low-velocity  $^{56}\text{Ni}$  must be responsible for the high peak and post-peak flux, which is above the early-time photometry by  $\sim 0.3$  mag, although the LC matches the very late photometry, as it should by design, since the inner distribution of  $^{56}\text{Ni}$  was obtained from fitting the nebular spectra. Moreover, there are only  $\approx 0.002M_{\odot}$  of  $^{56}\text{Ni}$  above  $10,000 \text{ km s}^{-1}$ , not enough to power a very fast early LC rise.

The *dotted line* is the synthesized LC of a model without the density enhancement below  $5000 \text{ km s}^{-1}$  and with the  $^{56}\text{Ni}$  distribution constrained by spectral modeling. The total ejecta mass, kinetic energy, and  $^{56}\text{Ni}$  mass are  $\approx 3.9M_{\odot}$ ,  $\approx 5 \cdot 10^{51}$  erg, and  $\approx 0.12M_{\odot}$ , respectively. Although the energy available is smaller, the LC peak is actually as bright as in the other models because less ejecta material is heated. However, because of the small ejecta mass relative to the kinetic energy, the LC peak is too narrow and the LC drops too rapidly when compared to the observations. As a further test of our model, we plot in the

*inset* of Fig. 5 the evolution of the photospheric velocity of the three models as estimated approximately by the LC code. They all reproduce well the values that were determined by spectral modeling (*stars*).

While we cannot exclude the possibility that other  $^{56}\text{Ni}$  distributions, with some tuning, may also give a good LC fit, it would be a futile attempt to try to pin down the  $^{56}\text{Ni}$  distribution so precisely in a one-dimensional model. Nonetheless, the distribution we adopted results in a rapid LC rise, and in a maximum luminosity and a broad LC peak that match the observations well. After about day 150 the model LC lies below the observations by  $\sim 0.2$  mag, but the slope is comparable.

## 5. Discussion

The properties of SN 2003bg derived from our analysis suggest that the SN was the explosion of a massive star, clearly more massive than the Type IIb SN 1993J. The large explosion energy ( $E_K \approx 5 \cdot 10^{51}$  erg) qualifies SN 2003bg as a hypernova, in line with the broad lines detected in the earliest spectra. If the ejected mass was  $\sim 4 - 5 M_\odot$ , of which  $\sim 1 - 2 M_\odot$  were He and only  $\sim 0.05 M_\odot$  was H, the star had lost only its H envelope. Assuming that the compact object formed at the time of core-collapse had a mass between  $1.4 M_\odot$  (if it was a neutron star) and  $2 M_\odot$  (if it was a black hole), we have a He star of  $\sim 5.5 - 7 M_\odot$  at explosion. This would imply a CO core of  $\sim 4 - 5 M_\odot$  and a star of main-sequence mass  $M_{ZAMS} \sim 22 - 25 M_\odot$ , very similar to the star that exploded as SN 2002ap (Mazzali et al. 2006) and also similar to, or perhaps somewhat less massive than the progenitor of the XRF-SN 2008D (Mazzali et al. 2008; Tanaka et al. 2009). SN 2003bg had a similar explosion energy as these two other SNe, but because of the larger  $M_{ej}$  very high velocities were not reached, and spectral lines were not as broad. This situation (low velocities, larger overlying mass) also would have made the generation of a hard X-ray or  $\gamma$ -ray transient very unlikely.

The  $^{56}\text{Ni}$  distribution derived from the light curve model is different from that obtained from the spectra. Most of the  $^{56}\text{Ni}$  obtained from the spectral models is required to power the nebular spectra. If a higher abundance of  $^{56}\text{Ni}$  was used outside of the  $5000 \text{ km s}^{-1}$  zone sampled by the nebular spectra, the synthetic [O I] 6300Å line would be too broad, unless  $^{56}\text{Ni}$  and oxygen were physically separated. This would be a signature of asymmetry in the explosion, as was seen in, e.g. , SN 1998bw (Mazzali et al. 2001).

SN 2003bg falls on the relations between stellar main sequence mass and, respectively, mass of  $^{56}\text{Ni}$  synthesised and  $E_K$  produced in the explosion (Nomoto et al. 2005), as shown in Figures 6 and 7, suggesting that these relations hold not only for SNe Ic but also for less



stripped core-collapse SNe.

Given our estimate of the progenitor mass, the compact remnant is likely to have been a black hole, but it also could have been a neutron star. Overenergetic explosions are expected also in this case if the neutron star is a magnetar (Bucciantini et al. 2008).

However, the presence of significant CSM gave rise to strong radio emission in SN 2003bg (Soderberg et al. 2006). What is the difference between SN 2003bg and SN 2006aj? SN 2006aj had lost its He envelope, and possibly part of its CO core. Thus the circumstellar material inside of which SN 2006aj exploded was composed mostly of oxygen (Mazzali et al. 2006) SN 2003bg only lost most of its H envelope, and H was the main constituent of the CSM (Soderberg et al. 2006). Quite possibly, SN 2006aj was a binary star, which helped ejecting the envelope. SN 2003bg may have been a single star, and if it was an interacting binary the effect of interaction was not as dramatic as in SN 2006aj.

PAM acknowledges support from contracts ASI-INAF I/023/05/0, ASI I/088/06/0, and PRIN INAF 2006. JD acknowledges partial support by the National Natural Science Foundation of China (Grant No. 10673014) and by the National Basic Research Program of China (Grant No. 2009CB824800). MH acknowledges support provided by NASA through Hubble Fellowship grant HST-HF-01139.01-A (awarded by the Space Telescope Science Institute, which is operated by the Association of Universities for Research in Astronomy, Inc., for NASA, under contract NAS 5-26555), the Carnegie Postdoctoral Fellowship, FONDECYT through grant 1060808, the Millennium Center for Supernova Science through grant P06-045-F (funded by “Programa Bicentenario de Ciencia y Tecnología de CONICYT” and “Programa Iniciativa Científica Milenio de MIDEPLAN”), Centro de Astrofísica FONDAF 15010003, and Center of Excellence in Astrophysics and Associated Technologies (PFB 06). This research has been supported in part World Premier International Research Center Initiative (WPI Initiative), MEXT, Japan, by the Grant-in-Aid for Scientific Research of the JSPS (18104003, 18540231, 20540226) and MEXT (19047004, 20040004).

## REFERENCES

- Abbott, D. C., & Lucy, L. B. 1985, *ApJ*, 288, 679
- Anupama 2005, *ApJ*, 631, L125
- Arnett, W. D. 1982, *ApJ*, 253, 785
- Axelrod, T.S. 1980 *Ph. D. Thesis, University of California, Santa Cruz*
- Branch, D., et al. 2002, *ApJ*, 566, 1005

- Bucciantini, N., Quataert, E., Arons, J., Metzger, B. D., Thompson, T. A. 2008, MNRAS383, L25
- Campana, S., et al. 2006, Nature, 442, 1008
- Clocchiatti, A., & Wheeler, J.C. 1997, ApJ, 491, 375
- Crockett, R. M., et al. 2008, MNRAS, 391, L5
- Deng, J, Qiu, Y., Hu, J, Hatano, K., & Branch, D. 2000, ApJ, 540, 452
- Filippenko, A.V., ARA&A, 35, 309
- Filippenko, A.V., et al. 1995, ApJ, 450, L11
- Filippenko, A.V., & Chornock, R. 2003, IAUC 8084, 4.
- Fryer, C. L. 1999, ApJ, 522, 413
- Galama, T.J., et al. 1998, Nature, 395, 670
- Ghisellini, G., Ghirlanda, G., & Tavecchio, F., 2007, MNRAS, 382, L77
- Gómez-Gomar, J., Isern, J., 1996, ApJ, 470, 1018
- Hamuy, M., et al. 2002, AJ, 124, 417
- Hamuy, M., et al. 2009, ApJ, submitted
- Heger, A., Fryer, C.L., Woosley, S.E., Langer, N., & Hartmann, D.H. 2003, ApJ, 591, 288
- Heise, J., in't Zand, J., Kippen, R.M., & Woods, P. M. 2001, Gamma-ray Bursts in the Afterglow Era, 16
- Iwamoto, K., Nomoto, K., Hoflich, P., Yamaoka, H., Kumagai, S., Shigeyama, T., 1994, ApJ, 437, L115
- Iwamoto, K., et al. 1998, Nature, 395, 672
- Iwamoto, K., et al. 2000, ApJ, 534, 660
- Leonard, D., et al. 2006, Nature, 440, 505
- Lucy, L.B. 1991, ApJ, 383, 308
- Lucy, L.B. 1999, A&A, 345, 211

- MacFadyen, A. I., & Woosley, S. E. 1999, *ApJ*, 524, 262
- Maeda, K., & Nomoto, K. 2003, *ApJ*, 598, 1163
- Maeda, K., Nakamura, T., Nomoto, K., Mazzali, P. A., Patat, F., & Hachisu, I. 2002, *ApJ*, 565, 405
- Maeda, K., et al. 2008, *Science*, 319, 1220
- Magee, N.H., et al., 1995, in Adelman, S.J., Wiese, W.L., eds, *ASP Conf. Ser. 78.*, *Astrophysical Applications of Powerful New Database*. ASP, San Francisco, p51
- Matheson, T., et al. 2003, *ApJ*, 599, 394
- Maund, J.R., Smartt, S. J., Kudritzki, R. P., Podsiadlowski, Ph., & Gilmore, G.F. 2004, *Nature*, 427, 129
- Mazzali, P.A. 2000, *A&A*, 363, 705
- Mazzali, P.A., Iwamoto, K., & Nomoto, K. 2000, *ApJ*, 545, 407
- Mazzali, P.A., & Lucy, L.B. 1993, *A&A*, 279, 447
- Mazzali, P.A., & Lucy, L.B. 1998, *MNRAS*, 295, 4287
- Mazzali, P.A., et al. 2002, *ApJ*, 572, L61
- Mazzali, P.A., Deng, J., Maeda, K., Nomoto, K., Filippenko, A.V., & Matheson, T. 2004, *ApJ*, 614, 858
- Mazzali, P.A., Nomoto, K., Patat, F., & Maeda, K. 2001, *ApJ*, 547, 988
- Mazzali, P.A., et al. 2005, *Science*, 308, 1284
- Mazzali, P.A., et al. 2006, *Nature*, 442, 1018
- Mazzali, P.A., et al. 2007, *ApJ*, 670, 592
- Mazzali, P.A., et al. 2008, *Science*, 321, 1185
- Nomoto, K., Suzuki, T., Shigeyama, T., Kumagai, S., Yamaoka, H., Saio, H. 1993, *Nature* 364, 507
- Nomoto, K., Yamaoka, H., Pols, O. R., van den Heuvel, E. P. J., Iwamoto, K., Kumagai, S., & Shigeyama, T. 1994, *Nature*, 371, 227

- Nomoto, K., Iwamoto, K., & Suzuki, T. 1995, *Phys. Rep.*, 256, 173
- Nomoto, K., and Hashimoto, M. 1988, *Phys. Rep.* 163, 13
- Nomoto, K., Mazzali, P. A., Nakamura, T., Iwamoto, K., Danziger, I. J., & Patat, F. 2001, in M. Livio, et al. (eds.), *Supernovae and Gamma-Ray Bursts: the Greatest Explosions since the Big Bang*, (Cambridge: Cambridge Univ. Press), 144
- Nomoto, K., Tominaga, N., Umeda, H., Maeda, K., Ohkubo, T., Deng, J. 2005, *Ap&SS*, 298, 81
- Patat, F., Chugai, N., & Mazzali, P. A. 1995, *A&A*, 299, 715
- Pauldrach, A. W. A., Duschinger, M., Mazzali, P. A., Puls, J., Lennon, M., & Miller, D. L. 1996, *A&A*, 312, 525
- Pian, E., et al. 2006, *Nature*, 442, 1011
- Ruiz-Lapuente, P., & Lucy, L. B. 1992, *ApJ*, 400, 127
- Richmond, M. W., et al. 1996, *AJ*, 111, 327
- Ryder, S. D., Murrowood, C. E., & Stathakis, R. A. 2006, *MNRAS*, 369, L32
- Sauer, D., et al. 2006, *MNRAS*, 369, 1939
- Silverman, J., et al. 2009, *ApJ*, in press [arXiv:0903.4179]
- Smith, N., & Conti, P. S. 2008, *ApJ*, 679, 1467
- Soderberg, A. M., Nakar, E., Berger, E., & Kulkarni, S. R. 2006, *ApJ*, 638, 930
- Soderberg, A. M., Chevalier, R., Kulkarni, S. R., & Frail, D. A. 2006, *ApJ*, 651, 1005
- Soderberg, A. M., et al. 2008, *Nature*, 453, 469
- Stockdale, C. J., Williams, C. L., Weiler, K. W., Panagia, N., Sramek, R. A., Van Dyk, S. D., & Kelley, M. T. 2007, *ApJ*, 671, 689
- Swartz, D. A., Sutherland, P. G., Harkness, R. P. 1995, *ApJ*, 446, 766
- Tanaka, M., et al. 2008, *ApJ*, 692, 1131
- Taubenberger, S., et al. 2006, *MNRAS*, 371, 1459
- Tominaga, N., et al. 2005, *ApJ*, 612, L105

Waxman, E., Mészáros, P., & Campana, S. 2007, *ApJ*667, 351

Weiler, K. W., Williams, C. L., Panagia, N., Stockdale, C. J., Kelley, M. T., Sramek, R. A.,  
Van Dyk, S. D., & Marcaide, J. M. 2007, *ApJ*, 671, 1959

Wheeler, J. C., Harkness, R. P., Clocchiatti, A., Benetti, S., Brotherton, M. S., Depoy, D. L.,  
& Elias, J. 1994, *ApJ*, 436, L135

Woosley, S., & Janka, T. 2005, *Nature Physics*, 1, 147

Table 1. Parameters of the early-time synthetic spectra

Date	SN epoch [days] <sup>a</sup>	$\log L$ [erg s <sup>-1</sup> ]	$v_{ph}$ km s <sup>-1</sup>	$f(\text{He I})$	$f(\text{H I})$
28 Feb 2003	3	41.47	22000	10 <sup>3</sup>	10 <sup>3</sup>
2 Mar 2003	5	41.82	18000	10 <sup>3</sup>	10 <sup>3</sup>
4 Mar 2003	7	41.95	14100	10 <sup>3</sup>	10 <sup>3</sup>
12 Mar 2003	15	42.31	8800	10 <sup>3</sup>	10 <sup>3</sup>
31 Mar 2003	34	42.29	6000	10 <sup>6</sup>	210 <sup>3</sup>
4 Apr 2003	38	42.24	5600	10 <sup>7</sup>	210 <sup>3</sup>
9 Apr 2003	43	42.21	5100	10 <sup>9</sup>	310 <sup>3</sup>
10 Apr 2003	44	42.20	5000	10 <sup>9</sup>	310 <sup>3</sup>

<sup>a</sup>The epoch is given from the putative date of explosion, 25 Mar 2003.

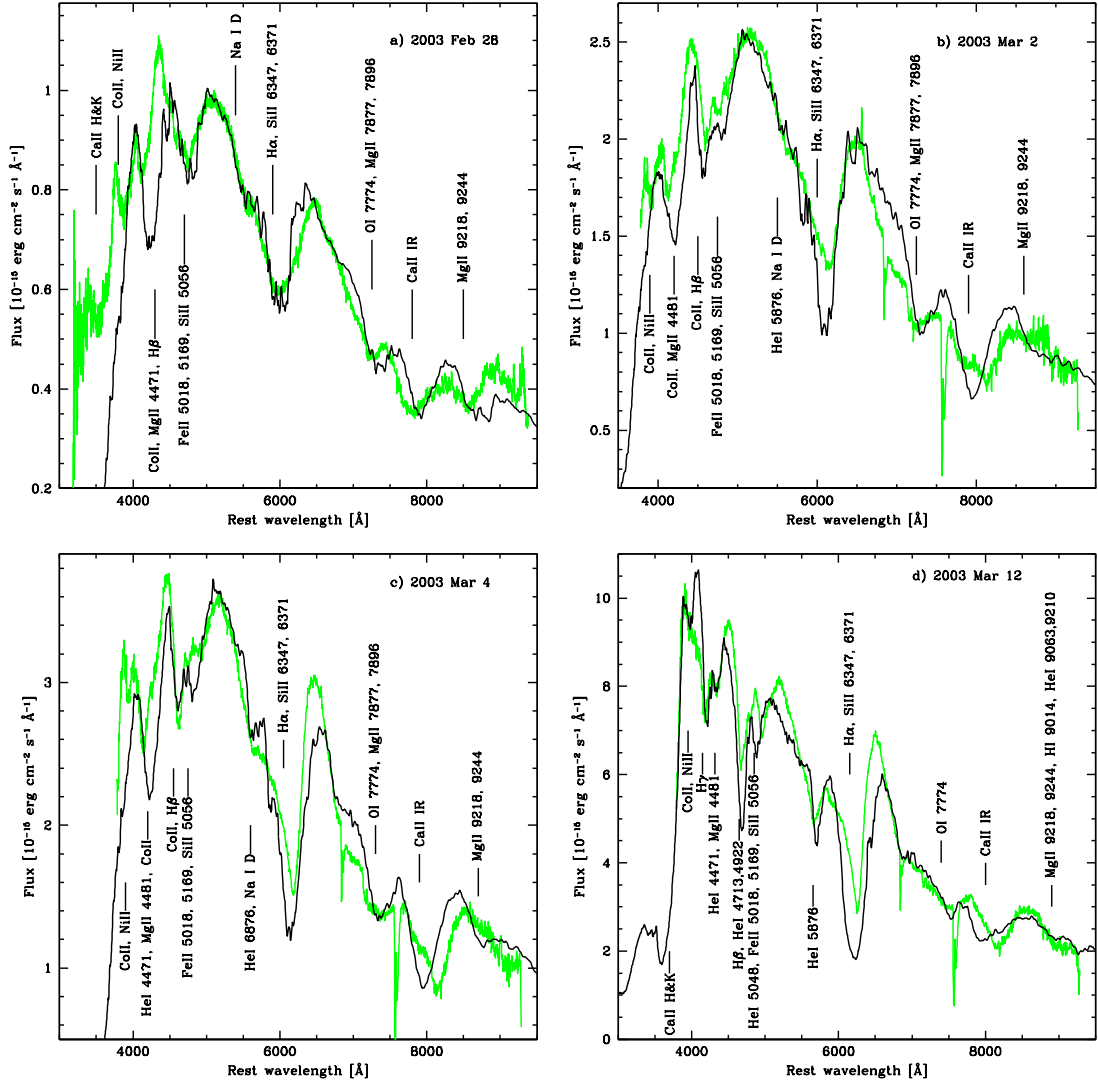


Fig. 1.— Observed spectra of SN 2003bg (green/black) compared to synthetic models (black/grey) for pre-maximum epochs.

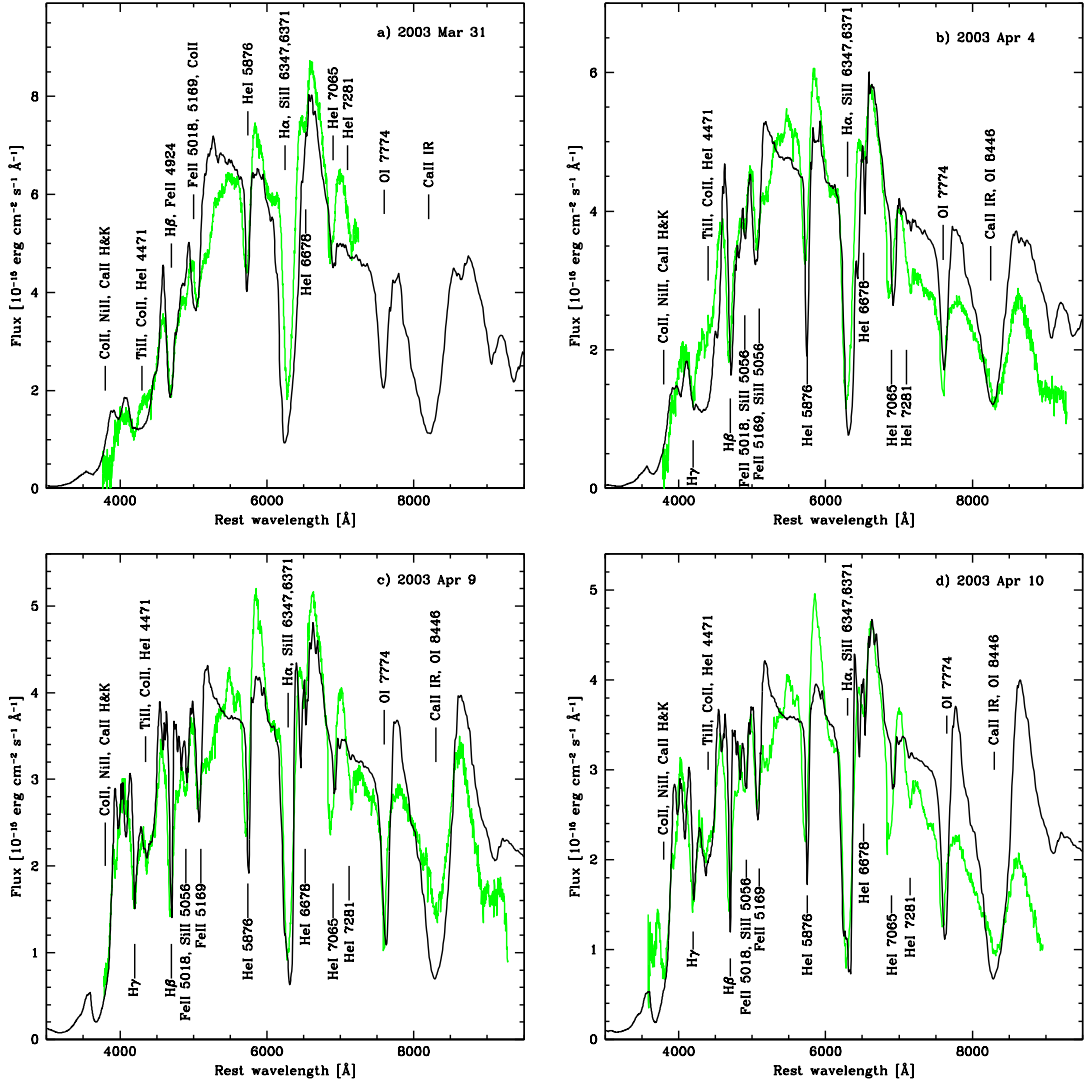


Fig. 2.— Observed spectra of SN 2003bg (green/black) compared to synthetic models (black/grey) for post-maximum epochs.



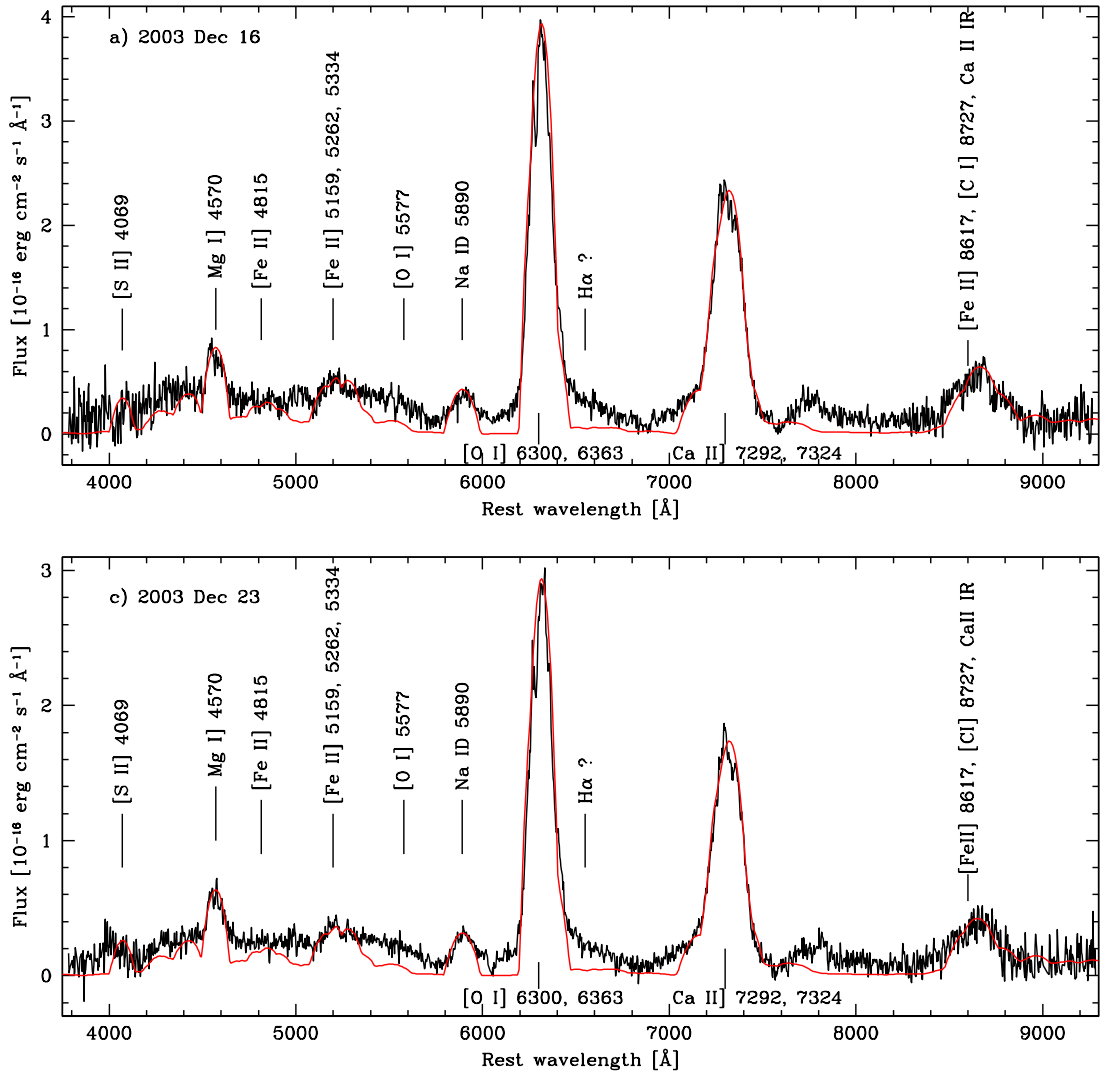


Fig. 3.— Observed nebular spectra of SN 2003bg (black) compared to synthetic models (red/grey).

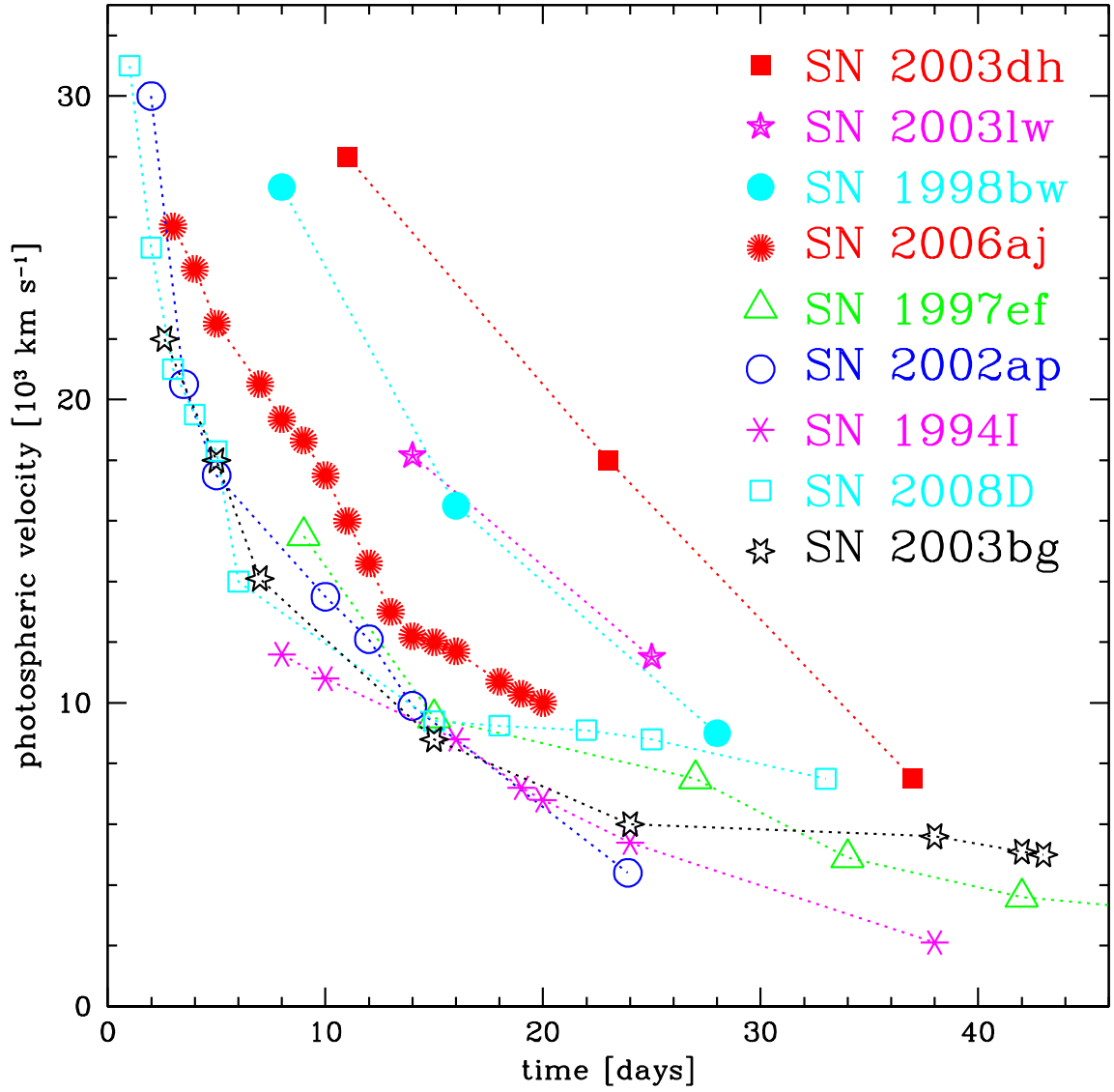


Fig. 4.— The evolution of the photospheric velocity obtained from spectral models in a number of SNe Ib/c.

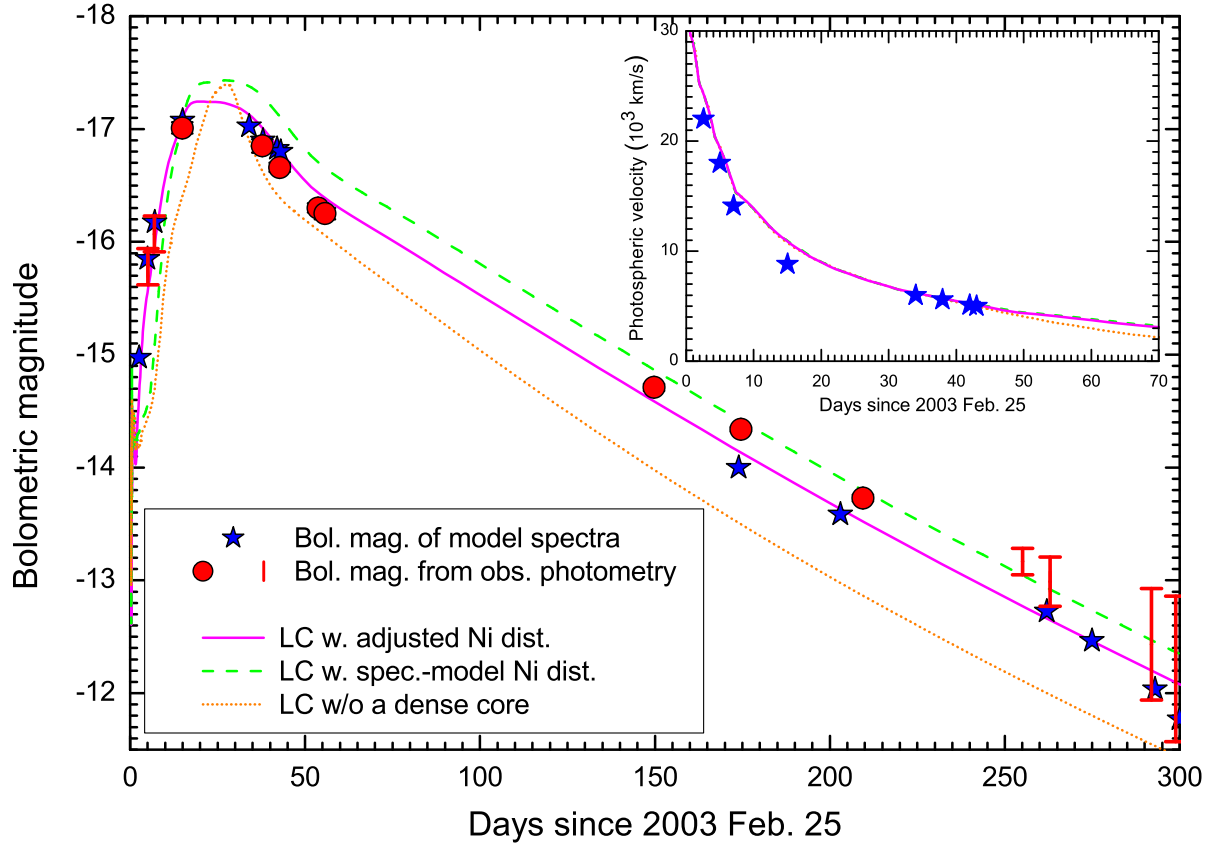


Fig. 5.— The bolometric light curve of SN 2003bg compared to the synthetic light curves of different models (see text). The inset shows the evolution of the photospheric velocity (as shown in Fig. 4) and the prediction of the various light curve models.

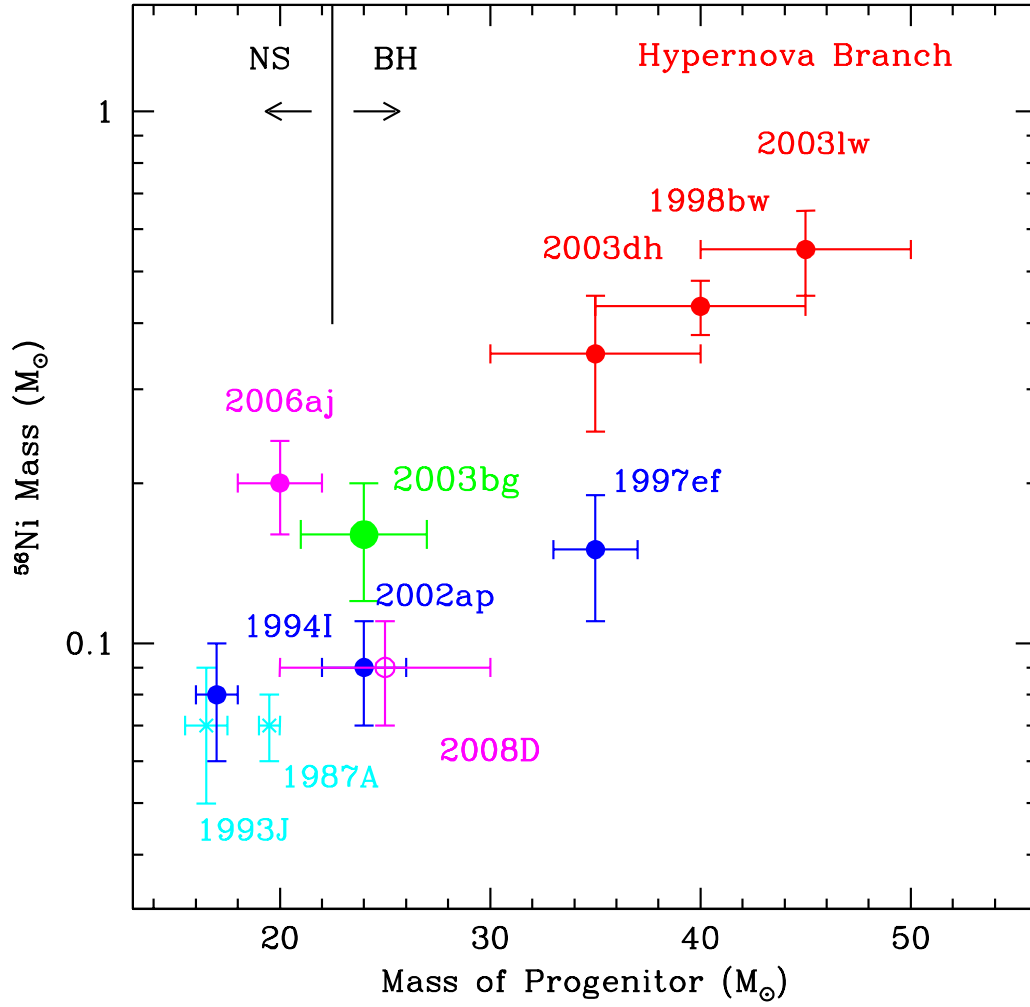


Fig. 6.— The relation between progenitor mass and synthesised  $^{56}\text{Ni}$  mass in a number of Type Ib/c SNe.

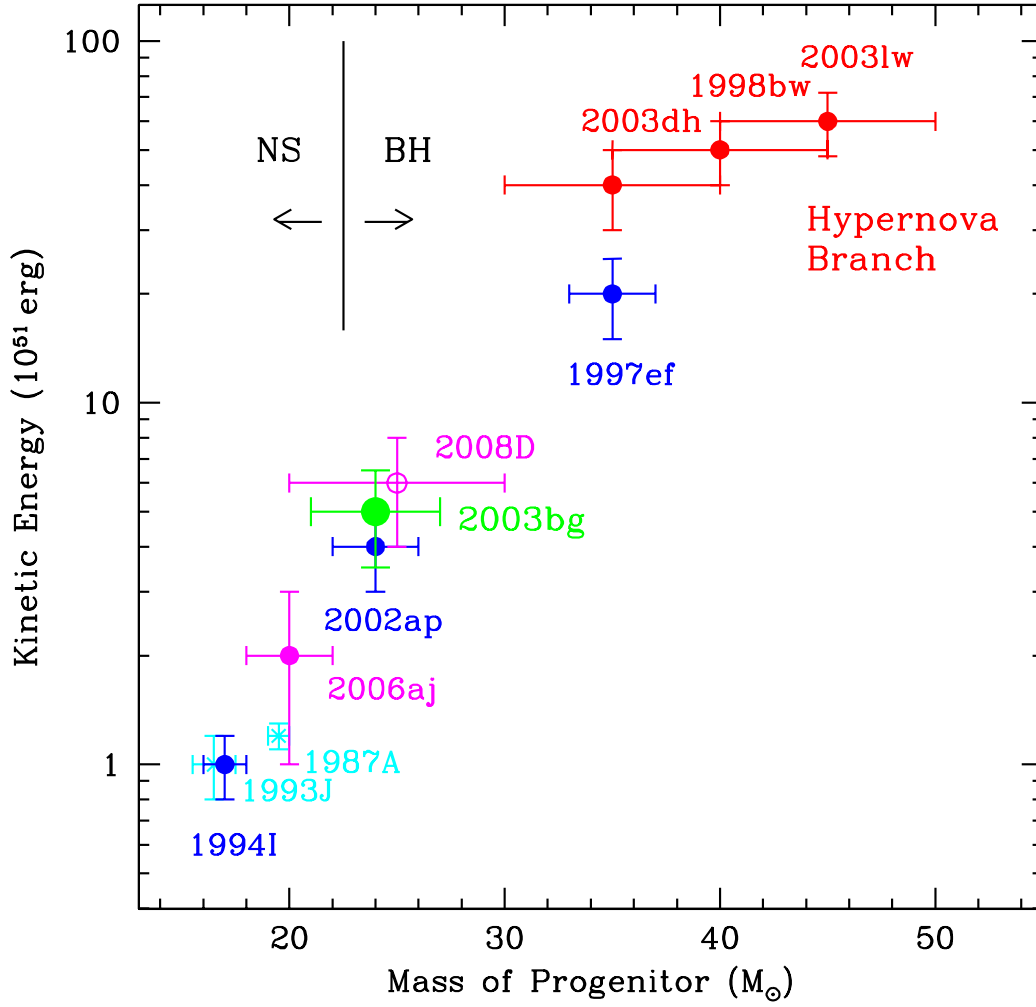


Fig. 7.— The relation between progenitor mass and explosion kinetic energy in a number of Type Ib/c SNe.